



HAL
open science

Correct stimulation of CD28H arms NK cells against tumor cells

Raphaëlle Leau, Pierre Duplouye, Virginie Huchet, Véronique Nerrière-Daguin, Bernard Martinet, Mélanie Néel, Martin Morin, Richard Danger, Cécile Braudeau, Régis Josien, et al.

► To cite this version:

Raphaëlle Leau, Pierre Duplouye, Virginie Huchet, Véronique Nerrière-Daguin, Bernard Martinet, et al.. Correct stimulation of CD28H arms NK cells against tumor cells. *European Journal of Immunology*, 2024, 54 (11), pp.e2350901. 10.1002/eji.202350901 . hal-04704026v2

HAL Id: hal-04704026

<https://hal.science/hal-04704026v2>

Submitted on 23 Jan 2025

HAL is a multi-disciplinary open access archive for the deposit and dissemination of scientific research documents, whether they are published or not. The documents may come from teaching and research institutions in France or abroad, or from public or private research centers.



L'archive ouverte pluridisciplinaire **HAL**, est destinée au dépôt et à la diffusion de documents scientifiques de niveau recherche, publiés ou non, émanant des établissements d'enseignement et de recherche français ou étrangers, des laboratoires publics ou privés.



Distributed under a Creative Commons Attribution - NonCommercial 4.0 International License

Research Article

Correct stimulation of CD28H arms NK cells against tumor cells

Raphaëlle Leau¹, Pierre Duplouye¹, Virginie Huchet¹,
Véronique Nerrière-Daguin¹, Bernard Martinet¹ , Mélanie Néel¹,
Martin Morin¹, Richard Danger¹, Cécile Braudeau^{1,2}, Régis Josien^{1,2},
Gilles Blancho¹ and Fabienne Haspot¹ 

¹ Center for Research in Transplantation and Translational Immunology, Nantes Université, CHU Nantes, INSERM, UMR 1064, Nantes, France

² CHU Nantes, Laboratoire d'Immunologie, CIMNA, Nantes, France

Tumor evasion has recently been associated with a novel member of the B7 family, HERV-H LTR-associating 2 (HHLA2), which is mostly overexpressed in PDL-1^{neg} tumors. HHLA2 can either induce a costimulation signal when bound to CD28H or inhibit it by binding to KIR3DL3 on T- and NK cells. Given the broad distribution of CD28H expression on NK cells and its role, we compared two monoclonal antibodies targeting this novel NK-cell engager in this study. We show that targeting CD28H at a specific epitope not only strongly activates Ca²⁺ flux but also results in NK-cell activation. CD28H-activated NK cells further display increased cytotoxic activity against hematopoietic cell lines and bypass HHLA2 and HLA-E inhibitory signals. Additionally, scRNA-seq analysis of clear cell renal cancer cells revealed that HHLA2⁺ clear cell renal cancer cell tumors were infiltrated with CD28H⁺ NK cells, which could be targeted by finely chosen anti-CD28H Abs.



Additional supporting information may be found online in the Supporting Information section at the end of the article.

Introduction

Immune checkpoint inhibitors (ICIs) of the B7 family, for example, anti-CTLA-4, anti-PD-1, and anti-PDL-1, have revolutionized oncotherapy in recent decades. However, some patients face primary or secondary resistance to ICI treatment, suggesting that tumor complexity and heterogeneity between and among patients need to be considered. A novel member of the B7 family, HERV-H LTR-associating 2 (HHLA2), was recently discovered in humans, but its absence in rodents has rendered it difficult to study.

HHLA2 was originally described as being expressed by epithelial cells of the colon, kidney, small intestine, and lung [1, 2], and its expression was found to be notably elevated in renal cancers [3]. Interestingly, clear cell renal cancer cells (ccRCC) express

either HHLA2 or PDL-1 but rarely both, in which case HHLA2⁺ and PDL-1⁺ cells do not overlap [4]. Like B7-1 and B7-2, HHLA2 has two receptors on immune cells: CD28H (also known as IGPR1 or TMIGD2) is the activating receptor [5, 6], while KIR3DL3 is the inhibitory receptor [4, 7]. CD28H is expressed in T-cells, NK cells, ILCs, and pDCs [5, 8], and it binds to the IgV1 domain of HHLA2 [7]. Demonstrating KIR3DL3 protein expression on T- and NK cells is challenging due to its little to no expression on circulating T- and NK cells [4, 9] and due to difficulties in obtaining reliable antibodies because of homologies between KIR proteins [4, 7, 9, 10]. However, KIR3DL3 expression can be detected on some modified NK92 cells (i.e. NK92-MIs) [4, 7]. Interestingly, KIR3DL3 and CD28H can simultaneously bind HHLA2 at different epitopes [7]. Several antibodies with inhibitory or activator

Correspondence: Dr. Fabienne Haspot
e-mail: fabienne.haspot@univ-nantes.fr

Raphaëlle Leau and Pierre Duplouye contributed equally to this work.

functions have been developed to target these novel molecules [4, 5, 7, 11], and the CD28H-extracellular portion has been used to develop CAR-NK cells [6, 12].

Considering the broad distribution of CD28H on circulating NK cells and its role, we hypothesized that anti-CD28H immunotherapy would boost the functions of NK cells. This strategy is advantageous compared with that of the recently described CD28H-CAR-NKL, whose effect is restricted to HHLA2-positive tumor cells. In this study, we compared two anti-CD28H monoclonal antibodies (mAbs) and demonstrated that targeting CD28H at the correct epitope not only strongly activated Ca^{2+} flux but also resulted in NK-cell activation. CD28H-activated NK cells display increased cytotoxic activity against hematopoietic cell lines and bypass HHLA2 and HLA-E inhibitory abilities. Finally, single-cell RNA sequencing (scRNA-seq) analysis of primary ccRCCs and adjacent tissues [13] revealed that HHLA2⁺ ccRCC tumors are infiltrated by CD28H⁺KIR3DL3^{neg} NK cells, which could be targeted with a finely selected anti-CD28H mAb.

Results

Targeting CD28H on NK cells with an agonistic mAb induces Ca^{2+} flux and gene regulation

CD28H is highly expressed in T- and NK cells [5]. To investigate the impact of CD28H trigger on NK cells, we compared two mAbs: one (clone 4–5) obtained from Dr. Cheng, known to activate T-cells [5], and the other from R&D Systems, described as blocking the CD28H/HHLA2 interaction. As shown by Blitz analysis, the anti-CD28H antibody from R&D efficiently blocks HHLA2 binding to CD28H (Fig. 1A), while the slight decrease in HHLA2/CD28H binding observed in the presence of anti-CD28H clone 4–5 is likely due to steric hindrance (Fig. 1A). This suggests that the two mAbs target different epitopes. Activating different NK-cell receptors on resting NK cells with mAbs has been shown to differentially mobilize intracellular Ca^{2+} flux [14]. Without cross-linking, none of the anti-CD28H mAbs alone were able to induce Ca^{2+} flux (Supporting Information Fig. S1B). Once cross-linked, the agonistic anti-CD28H mAb induces strong Ca^{2+} flux, while the cross-linking of the blocking anti-CD28H mAb does not (Fig. 1B, Supporting Information Fig. S1B). Therefore, targeting CD28H with mAbs that bind to different epitopes does not induce similar intracellular consequences, suggesting that all anti-CD28H mAbs do not act similarly on NK cells. Next, we evaluated each anti-CD28H mAb in combination with anti-CD16 or anti-NKp46. Indeed, the blocking anti-CD28H mAb has a synergistic effect when used together with anti-NKp46 or anti-CD16 in the P815 redirected cytotoxicity assay [6]. The Anti-CD16 antibody alone induces a small Ca^{2+} flux, which further increases after cross-linking with a secondary antibody (Supporting Information Fig. 1C), confirming published results [14]. The overall Ca^{2+} flux induced by the agonistic anti-CD28H mAb was as potent as that induced by the anti-CD16 or anti-NKp46 antibody (Fig. 1C and D). The cocrosslinking of CD16 and CD28H receptors did not result in a synergistic effect

(Fig. 1C), while the cocrosslinking of NKp46 and CD28H receptors with the agonistic mAb resulted in a significant increase in Ca^{2+} flux (Fig. 1D, Supporting Information Fig. S1D). Notably, the cocrosslinking of NKp46 and CD28H with the blocking anti-CD28H mAb did not result in an increase in Ca^{2+} flux compared with that of anti-NKp46 alone (Fig. 1D). Therefore, the anti-CD28H clone 4–5 is superior to the blocking anti-CD28H mAb in eliciting Ca^{2+} flux upon crosslinking.

Given the strong Ca^{2+} flux observed after CD28H crosslinking with the agonistic mAb, we next investigated the functional consequences of such stimulation. The transcriptional signature of bulk NK cells was analyzed after overnight culture with the agonistic anti-CD28H antibody or the isotype control. A comparison of gene expression between the two conditions revealed 216 significantly differentially expressed genes (DEGs), 108 of which showed upregulated expression and 108 of which showed downregulated expression (Fig. 1E). We analyzed gene ontology (GO) enrichment related to biological processes associated with the DEGs in both groups. The GO terms for which most of the upregulated genes were enriched included positive regulation of cell adhesion, regulation of immune effector process or lymphocyte activation, positive regulation of external processes, and T-cell differentiation. Conversely, the GO terms for which most of the downregulated genes were enriched included leukocyte migration, neutrophil activation, positive regulation of secretion, and cytokine production (Fig. 1F). Interestingly, *TNFRSF9* (4-1BB), *CRTAM* [15], *IL2RA*, and *IRF4* expression were highly upregulated, revealing increased NK-cell activation and effector functions upon CD28H triggering (Fig. 1G) [16, 17]. Additionally, we performed FACS analysis to evaluate the expression of activation markers on NK cells cultured overnight with the agonistic anti-CD28H mAb. We observed a decrease in CD16 expression compared with that in the isotype control group (Fig. 1H). NK-cell activation is known to result in the shedding of CD16A expression by ADAM17 regardless of CD16 engagement during this activation [18]. The expression of CD69, Tim-3 [19], and 4-1BB (*TNFRSF9*) was significantly upregulated following anti-CD28H treatment (Fig. 1H), confirming the NK-cell activation status observed in the bulk RNA-seq data (Fig. 1G).

In conclusion, when correctly targeted with mAbs, the CD28H receptor alone contributes to a signal in resting NK cells that results in increased Ca^{2+} mobilization and in the regulation of gene expression profiles that suggest the activation of NK cells.

CD28H-activated human NK cells exhibit increased effector functions

Since the results presented in Fig. 1 demonstrate that the anti-CD28H mAb clone 4–5 is superior to that from R&D Systems for activating NK cells, we next concentrated on analyzing NK-cell effector functions. We decided to maintain the setup that we developed for bulk RNA-seq analysis by activating NK cells overnight with the agonistic anti-CD28H antibody or the isotype control. Brefeldin A was added during the last 4 h of

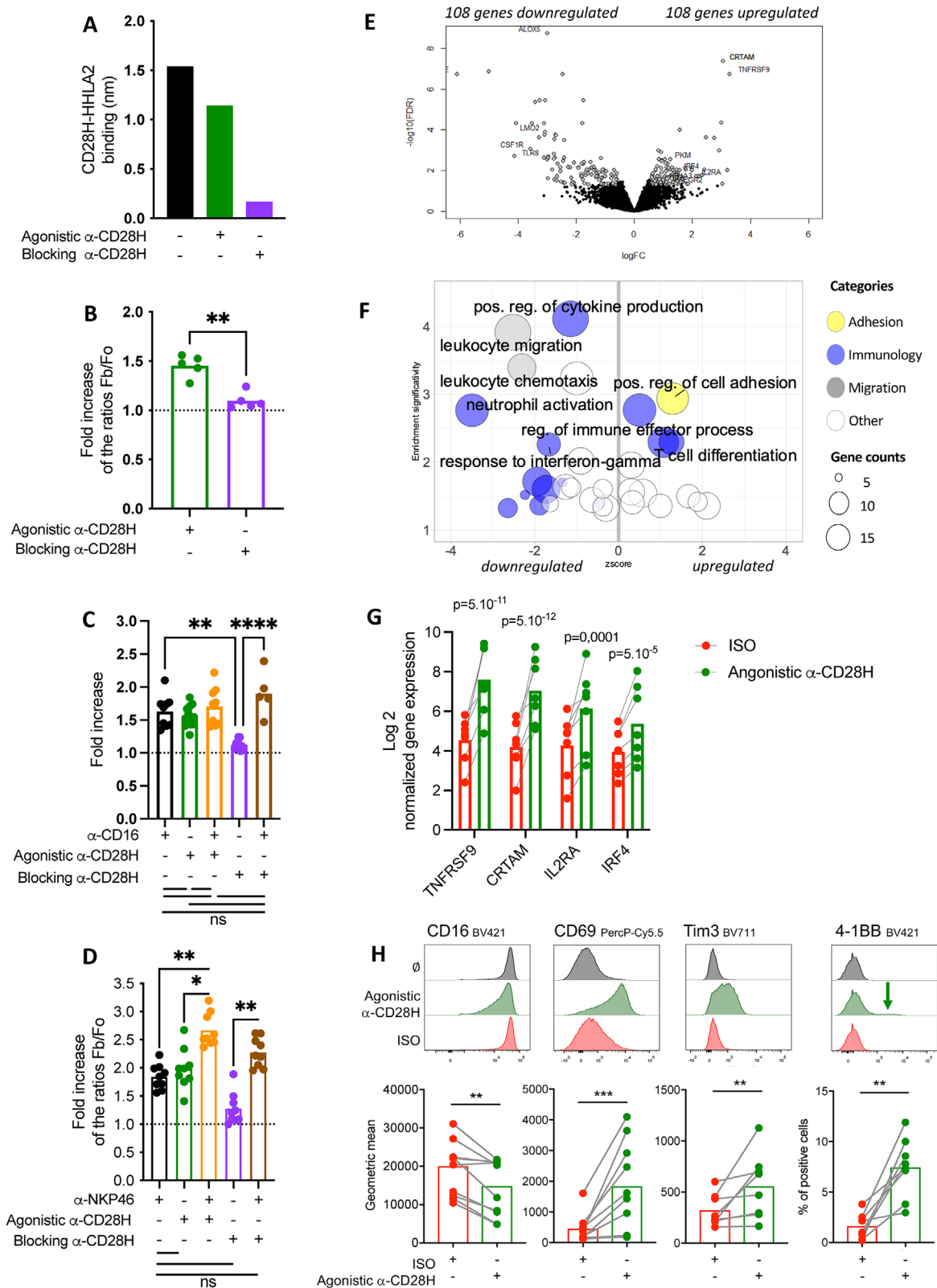


Figure 1. Triggering CD28H on NK cells with an agonistic mAb induces Ca^{2+} flux and differential gene expression. (A) Blitz analysis of the CD28H/HHLA2 interaction alone, in the presence of the agonistic anti-CD28H mAb (clone 4–5), or in the presence of the blocking anti-CD28H mAb (MAB8316). The binding affinity of HHLA2 for CD28H under each condition is presented. (B–D) Ca^{2+} flux is presented as the fold increase between the Fb/Fo ratio at 20 s and the Fb/Fo ratio at 180 s after the cross-linking of the indicated receptor combinations; $n = 5–9$ independent experiments. Nonsignificant differences (ns) are shown under the graph for ease of reading. The means are presented, and each symbol represents an HD

incubation, and NK cells were then intracellularly stained using anti-IFN- γ . We observed that CD28H activation with the agonistic anti-CD28H mAb resulted in a significant increase in IFN- γ^{pos} NK cells compared with NK cells incubated overnight with the isotype control, confirming that CD28H stimulation activated NK cells (Fig. 2A). We next hypothesized that this priming would lead to increased NK-cell function toward K562 cells, a chronic myelogenous leukemia cell line that does not express HLA class I. Indeed, NK cells primed with the agonistic anti-CD28H mAb were more potent at producing IFN- γ than ISO-treated NK cells, as shown by the intracellular analysis of IFN- γ^+ -producing NK cells (Fig. 2B). A significantly greater amount of secreted IFN- γ was also detected in the supernatant after 6 h of coculture with K562 cells (Fig. 2C). The secretome of NK cells activated with the agonistic anti-CD28H mAb overnight and subsequently cocultured with K562 cells revealed increased concentrations of cytotoxic molecules such as granzymes A, B (GZM), and FAS-L. Notably, NK cells activated with the blocking anti-CD28H mAb overnight and subsequently cocultured with K562 cells failed to secrete such soluble factors (Fig. 2D). There was no synergistic effect when anti-NKp46 and the agonistic anti-CD28H mAb were used to activate NK cells prior to their coculture with K562 cells (Supporting Information Fig. S2). Taken together, these data suggest that stimulation of CD28H results in an increase in natural NK-cell cytotoxicity against K562 target cells. These results indicate that pretreatment with the agonistic anti-CD28H mAb primes NK cells and leads to the secretion of cytotoxic molecules when primed NK cells are subsequently cocultured with target cells. Importantly, overnight stimulation with the agonistic anti-CD28H mAb or the blocking anti-CD28H mAb did not lead to the internalization of the targeted molecule. Indeed, after overnight stimulation with the agonistic mAb, CD28H molecules remained at the cell surface and were still fully bound by the agonistic anti-CD28H clone 4–5 mAb (Supporting Information Fig. S3A and B). We performed a similar experiment with the blocking mAb and observed a different staining profile, which might be due to the different affinities of the blocking mAb as compared with the agonistic mAb and/or to the secondary mAb, which was labeled with a less bright fluorochrome. Less CD28H staining was observed after overnight incubation with this antibody, yet CD28H expression was not completely absent. Further investigations are required to evaluate whether CD28H was internalized or whether another mechanism is responsible. Nevertheless, after overnight culture, most of the blocking mAb remained at the cell surface

with a low amount of CD28H molecules free of the mAb (although this difference was not significant) (Supporting Information Fig. S3C and D).

NK cells kill target cells through the Ca^{2+} -dependent release of lytic granules or by the secretion of cytotoxic molecules such as FAS-L through a Ca^{2+} -independent pathway [20]. Compared with isotype-treated NK cells, NK cells stimulated with the agonistic anti-CD28H mAb and subsequently cultured with K562 cells displayed increased cytotoxic potential, as evidenced by the accumulation of GZM A and GZM B expression and FAS-L expression in their supernatant. We then investigated the cytolytic function of CD28H-activated NK cells in a cytotoxic assay with calcein-labeled K562 target cells. An overnight culture of NK cells with the agonistic anti-CD28H mAb significantly increased their cytotoxicity against K562 target cells compared with NK cells cultured overnight either alone or with the blocking anti-CD28H mAb (Fig. 3A), which is consistent with their secretory function (Fig. 2D). Importantly, there was no significant difference in the cytotoxicity of CD16-activated NK cells to that of CD28H-activated NK cells at any of the E:T ratios except one (i.e. 10:1) (Fig. 3B). Although our results regarding Ca^{2+} flux indicate synergistic activity between CD28H and NKp46 (Fig. 1D), the observed secretory function in the presence of K562 cells does not support this observation (Supporting Information Fig. S3). Therefore, we evaluated the effects of NKp46 and CD28H coengagement on NK-cell lysis in K562 cells. Although the agonistic anti-CD28H mAb and the anti-NKp46 antibody overnight-treated NK cells had similarly elevated cytotoxicity against K562 cells, no synergistic effect was observed with the combination pretreatment (i.e. overnight stimulation with both mAbs; Fig. 3C). Notably, the blocking anti-CD28H mAb did not synergize with the anti-NKp46 antibody in this cytotoxicity assay (Fig. 3D).

CD28H-activated NK cells exhibit increased cytotoxicity not only against K562 cells but also against DAUDI and Jurkat cells (Supporting Information Fig. S4). In conclusion, we showed that NK cells exhibit increased cytotoxicity when an agonistic anti-CD28H mAb is used for activation.

Targeting CD28H bypasses some inhibitory signals sensed by NK cells

HHLA2 has dual functions depending on the receptor with which it engages. HHLA2 activates T- and NK cells when it binds to

analyzed in independent experiments. (E–G) NK cells from 6 different HDs were analyzed by bulk RNA-seq after overnight culture with the agonistic anti-CD28H mAb or the isotype control (ISO). (E) Volcano plot of the isotype control and anti-CD28H agonistic treatment groups. The 216 significant DEGs are represented by gray circles with some gene symbols. (F) Significantly enriched gene ontologies (GO) related to biological processes are presented, with the z score as a function of the adjusted *p*-value calculated with the clusterProfiler and GOplot R packages. The size of the dots indicates the number of genes, and the colors represent the four categories for ease of reading. (G) Normalized gene expression (trimmed mean of *M*-values-normalized cpm) in \log_2 of selected genes is represented for each HD, and adjusted *p*-values are depicted. (H) NK-cell activation markers are presented on representative histograms of overnight stimulated NK cells under the indicated culture conditions (upper panels). The first gate was set on physical parameters (FSC-SSC), and the second gate was set on CD56-positive cells. The geometric means of independent experiments are shown in the lower row, except for 4-1BB, for which the mean percentage of positive cells is shown; each symbol represents an HD analyzed in independent experiments. (B, H) Significance was calculated by the Wilcoxon matched pairs signed rank test (C, D) and the Friedmann test. ns: not significant; **p* < 0.05; ***p* < 0.01; ****p* < 0.001.

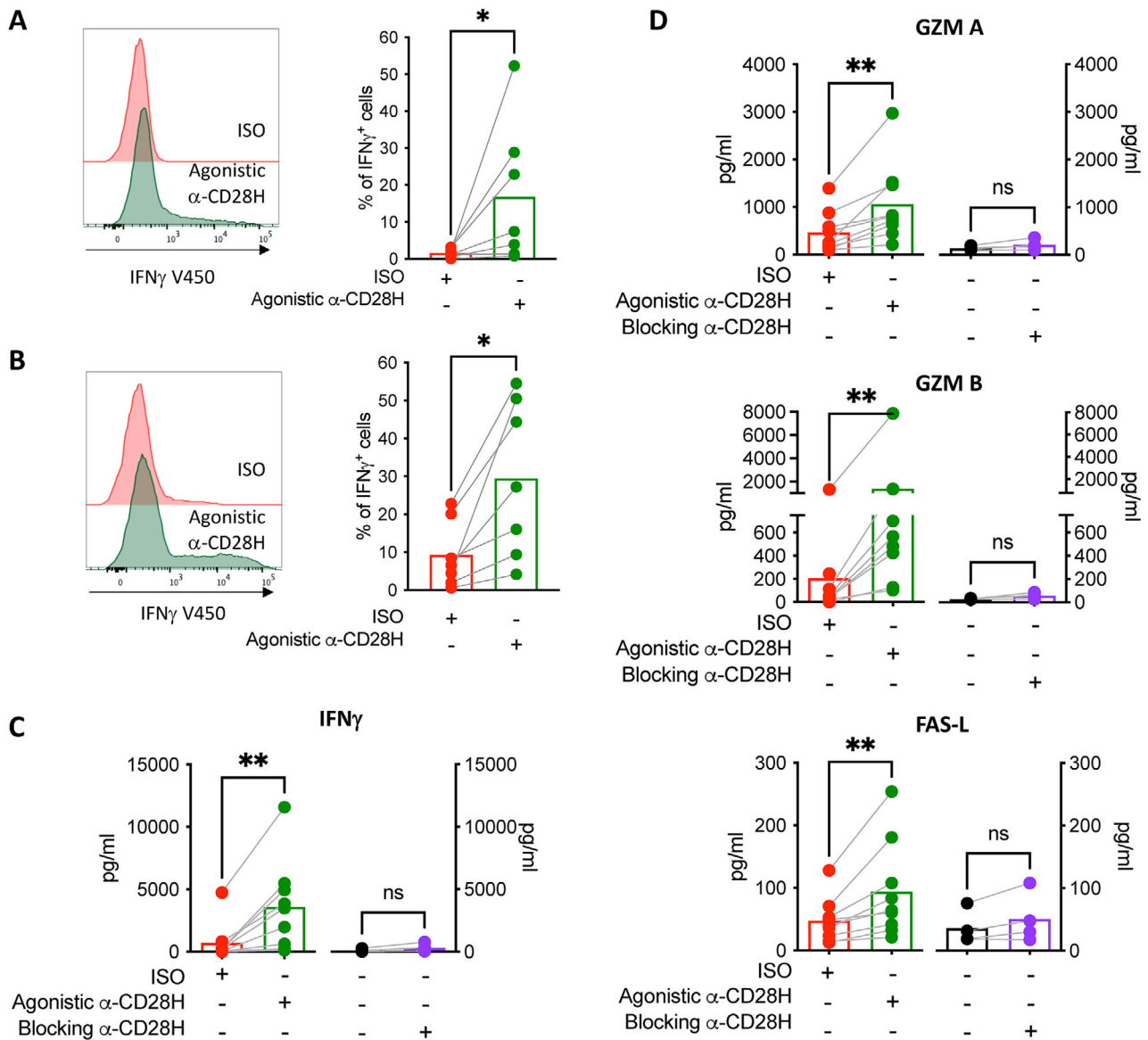


Figure 2. NK cells activated with the agonistic anti-CD28H mAb have increased secretion. (A) Freshly isolated NK cells cultured overnight with the indicated mAbs prior to treatment with brefeldin A for 4 h for FACS staining of intracellular IFN γ . NK cells were gated based on physical parameters (FSC-SSC). (B) Similar to (A), K562 cells added during the last 4 h of culture in the presence of brefeldin A. NK cells were gated based on physical parameters (FSC-SSC). (A, B) The percentage of IFN γ -positive NK cells is shown for 7 HDs, and the means are presented. Statistical analysis was performed by the Friedman test followed by Dunn's multiple comparison test. (C, D) Freshly isolated NK cells cultured overnight with agonistic or blocking anti-CD28H mAbs were then cultured for 6 h with K562 cells. The NK-cell secretome was analyzed by Luminex in the culture supernatant of four to nine independent experiments with different HDs. Significance was calculated by the Wilcoxon matched-pairs signed rank test, ** $p < 0.01$, ns not significant. The means are presented, and each symbol represents an HD.

CD28H [5, 6]. Conversely, HHLA2 inhibits T-cell activation and proliferation upon TCR and CD28 stimulation and suppresses NK-cell cytotoxic functions by interacting with its inhibitory receptor, which was recently identified to be KIR3DL3 [4, 7]. KIR3DL3 is a polymorphic molecule barely detectable by FACS [21]. To investigate the effects of HHLA2, we transduced K562 cells to express HHLA2 (K562-HHLA2 cells), which can bind recombinant CD28H-Fc and KIR3DL3-Fc proteins (Fig. 4A). When we loaded K562-HHLA2 cells with calcein, we noticed an increase in the passive release of calcein compared with that in WT K562 cells,

which could jeopardize the assay (data not shown). To prevent this possibility, we used a CD107a staining assay to assess NK-cell degranulation [22]. The results showed that NK-cell natural cytotoxicity was significantly decreased when target cells expressed HHLA2 (Fig. 4B). Importantly, this inhibition was reversed by CD28H stimulation with the agonistic mAb alone since CD28H-stimulated NK-cell cytotoxicity was restored to a level comparable to that observed in unmodified K562 WT target cells (Fig. 4B). This experiment was performed with NK cells directly stimulated by target cells in the presence or absence of anti-CD28H mAbs.

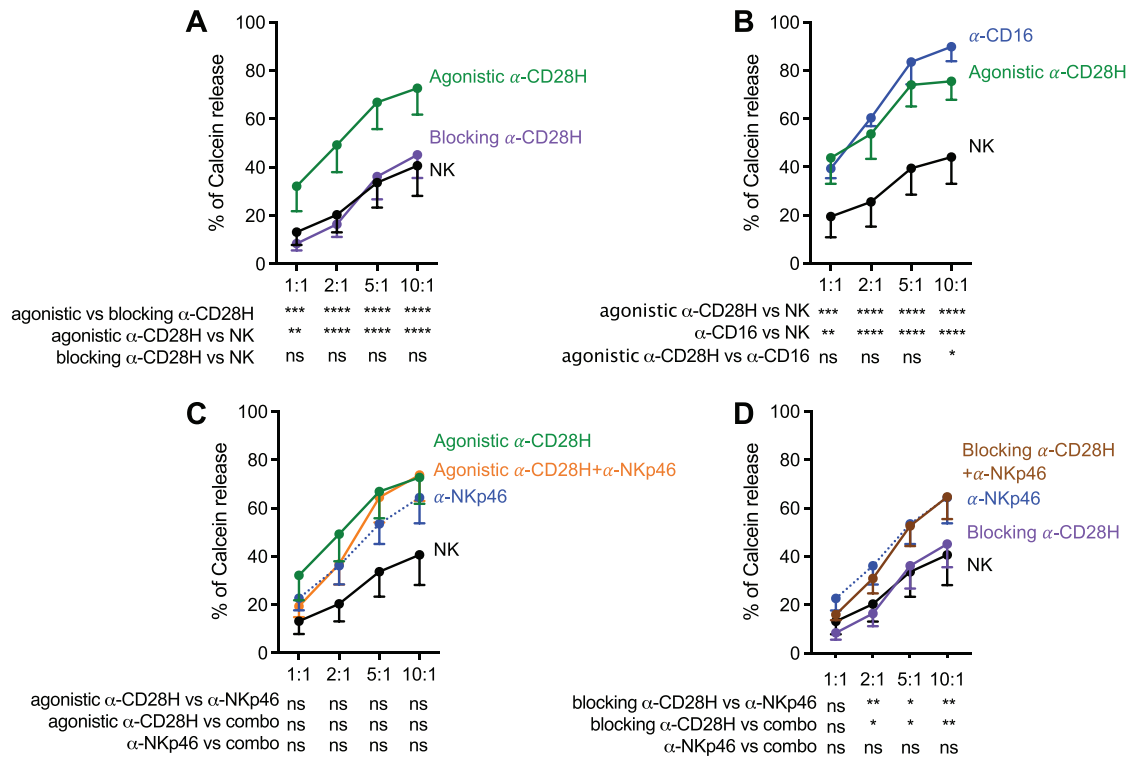


Figure 3. The agonistic anti-CD28H mAb increases NK-cell cytotoxic activity. (A–D) NK cells cultured overnight with the indicated mAbs were then plated for 4 h in the presence of calcein-labeled K562 target cells at the indicated E:T ratio (mean \pm SEM). Cytotoxicity against K562 target cells is presented as the percentage of calcein release. $n = 4$ to 5 independent experiments per graph. Significance was calculated by two-way ANOVA followed by Dunn's multiple comparisons test. ns: nonsignificant, * $p < 0.05$; ** $p < 0.01$; *** $p < 0.001$; **** $p < 0.0001$.

Within 2 h of culture stimulation, NK cells rapidly expressed the activation markers CD69 and TIM-3 but not CD16 (Supporting Information Fig. S5A–C). Importantly, the agonistic anti-CD28H mAb significantly increased NK-cell direct cytotoxicity compared with that induced by the blocking anti-CD28H mAb, regardless of HHLA2 expression on the K562 target cells (Supporting Information Fig. S5D), confirming the results obtained with overnight-primed NK cells (Fig. 4B).

When stably expressed with properly loaded peptides, HLA-E is a key player in tumor resistance against cytotoxicity by NK and CD8⁺ T-cells [23]. Thus, we exploited K562 cells modified to express both HLA-A2 and HLA-E (i.e. stably expressing HLA-E) and the control K562-HLA-A2 cells, which do not express HLA-E (Fig. 4C). As expected, there were significantly fewer K562-HLA-E⁺ cells killed by NKG2A⁺CD94⁺ NK cells than their control counterparts. Interestingly, NK cells that were stimulated overnight with the agonistic anti-CD28H mAb restored their cytotoxicity against K562-HLA-E⁺ cells to a level almost equivalent to that observed in unstimulated NK cells against the control target cells (Fig. 4D). These results clearly demonstrate that NK cells stimulated with an agonistic anti-CD28H mAb can bypass HHLA2 and HLA-E inhibitory signals, indicating that this strategy could still be efficient when targeting HHLA2⁺ or HLA-E⁺ tumor cells. This suggests that the use of an agonistic anti-CD28H mAb is a potential therapeutic approach in such cases.

Single-cell RNA sequencing of ccRCC tissues and adjacent tissues revealed the accumulation of a TMIGD2⁺ (CD28H) NK-cell cluster in the tumor

In a pancancer survival analysis, HHLA2 was shown to be overexpressed in multiple tumor types through transcriptomic analysis and was identified as an independent prognostic factor in 9 out of 20 human cancers, especially renal clear cell carcinoma [3]. Interestingly, HHLA2 was one of the B7 family members with the highest level of expression in ccRCC tissue compared with normal tissue, and half of ccRCC primary tumors analyzed by Bhatt and colleagues expressed HHLA2 but not PDL-1[4]. Thus, we reanalyzed an scRNA-seq public dataset (GSE178481) consisting of 15 primary ccRCC tissues and nine adjacent tissues [13] to investigate (1) HHLA2 and (2) CD28H expression in tumor- and NK cells (from tumor and adjacent tissues), respectively. Unsupervised clustering of the dataset revealed 21 distinct clusters annotated with the genes used by Alchahin et al. [13], with cluster 21 corresponding to tumor cells and cluster 15 corresponding to NK cells (Fig. 5A). Using the tumor cell signature in a study by Alchahin et al. [13], we confirmed that some tumor cells expressed *HHLA2* (Fig. 5B), while *TMIGD2*, which encodes CD28H, was expressed mainly by T-cells (clusters 1 and 4) and NK cells (cluster 15) (Fig. 5B). Further subcluster analysis of the NK cells revealed eight distinct clusters (Fig. 5C). *TMIGD2* was

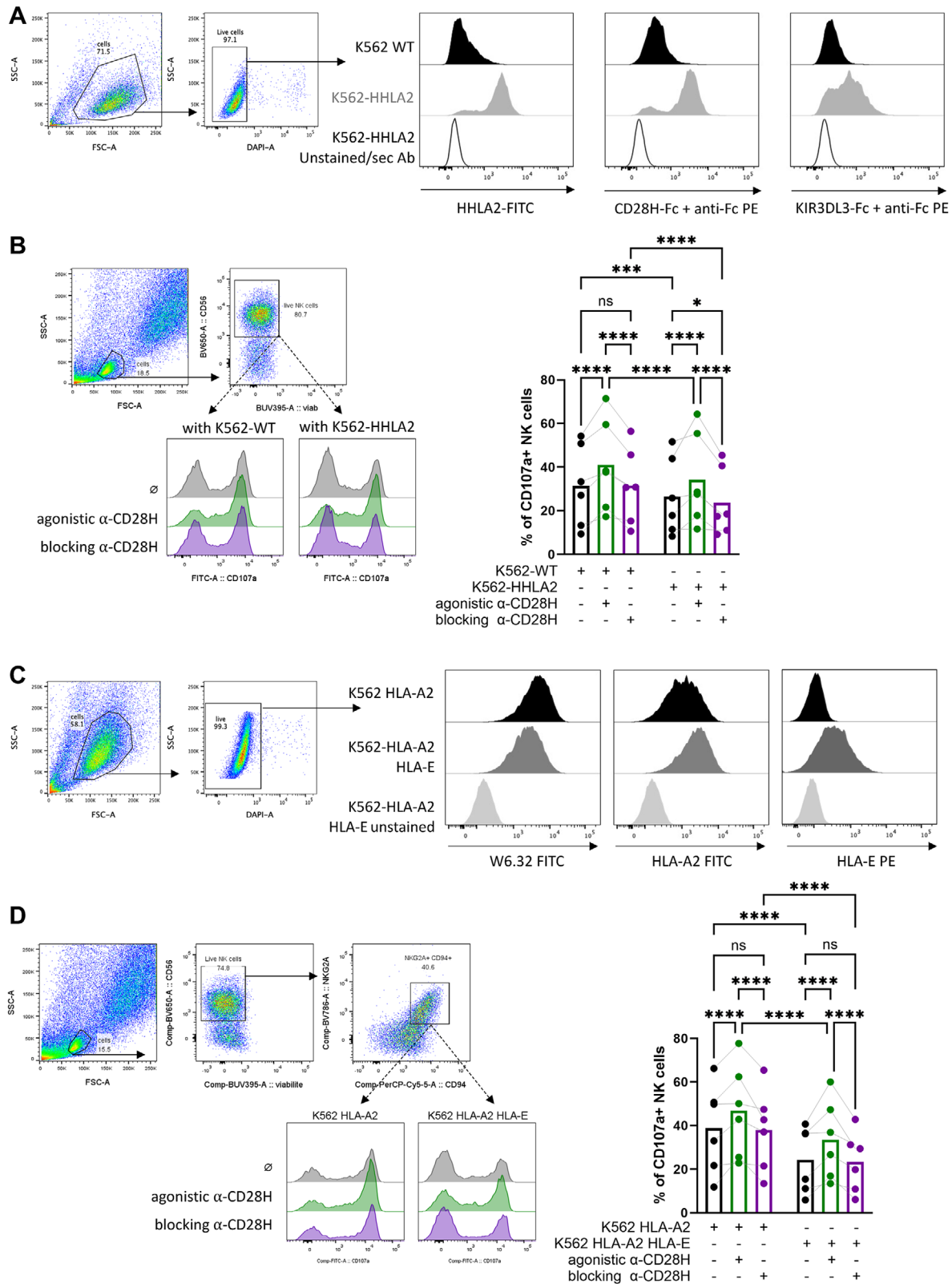


Figure 4. CD28H activation bypasses NK-cell inhibitory signals. (A) WT (black) and HHLA2-transduced (gray) K562 cells were analyzed by FACS for their expression of HHLA2 and for their ability to bind the CD28H-Fc and KIR3DL3-Fc proteins. (B) Freshly isolated NK cells were cultured overnight with the indicated mAbs prior to being seeded with the indicated target cells at a 1:2 E:T ratio. CD107a expression was analyzed by FACS. A representative FACS analysis is shown on the left. The percentages of CD107+ NK cells in 6 HDs from three independent experiments are shown. Significance was calculated by two-way ANOVA followed by Dunn's multiple comparisons test. ns: nonsignificant, * $p < 0.05$; ** $p < 0.01$; *** $p < 0.001$;

expressed in several of these clusters, with cluster 1 showing the highest intensity (Fig. 5C). Interestingly, TMIGD2^{pos} NK cells from adjacent and tumor tissues seemed to express TMIGD2 at similar levels (Fig. 5D, left panel). However, TMIGD2^{pos} NK cells were significantly more abundant in tumors (2190 TMIGD2^{pos} NK cells out of 12798 total NK cells, that is, 17%) than in adjacent tissues (425 TMIGD2^{pos} NK cells out of 3028 total NK cells, that is, 14%) (Fig. 5D, right panel). NK cells from cluster 1 were more enriched in tumor tissues than in adjacent tissues (21.07% vs. 8.62%, respectively, Fig. 5D, pie charts). These data may suggest that NK cells from cluster 1, which are overrepresented in tumor tissues, have greater migration capacity into tumors than NK cells from the other clusters and/or that the tumor microenvironment might promote their survival. The heatmap showing the expression of genes used to define immature, mature, and cytotoxic NK cells [24] highlights that NK cells from cluster 1 have a more immature profile regardless of their origin. Indeed, NK cells from cluster 1 expressed genes such as *KLRC1* and *NCAM1* (encoding CD56) and, in contrast, expressed low levels of mature NK genes (*B3GAT1*, *KIR3DL1*, *KIR2DL1*, *KIR2DL3*) or cytotoxic genes such as *PRF1*, *GNLY*, *GZMK*, *GZMH*, and *GZMB* (Fig. 5E). Interestingly, NK cells from cluster 1 in the tumor tissues expressed higher levels of *KLRC1* (encoding NKG2A) than did those from the adjacent tissues. In conclusion, tumor-infiltrating NK cells that express high levels of *TMIGD2* exhibit an immature NK-cell profile with a less-activated state and could hopefully be activated by an agonistic anti-CD28H antibody.

Discussion

NK-cell activation is controlled by the integration of signals from activating and inhibitory receptors potentially engaged by their ligands on target cells. Immunotherapies have been developed to finely tune immune cell activation against cancer cells, allowing receptor signaling even in the absence of ligands on tumor cells. Some strategies developed to enhance NK-cell functions (see [25, 26] for reviews) rely on the stimulation of activating receptors such as NKp46 [27] and NKp30 [28], while others target major NK-cell inhibitors such as NKG2a [29] and KIRs, including KIR3DL3 [4, 7]. In this study, we evaluated CD28H as a potential target for immunotherapy. Indeed, given its broad distribution on NK cells [5, 8] and its depicted role in T- and NK-cell activation [5, 6], we reasoned that targeting CD28H with a mAb would increase NK-cell function and offer promising antitumor activity even in the HHLA2^{neg} tumor microenvironment.

We compared the abilities of two anti-CD28H mAbs to initiate NK-cell activation. We first showed that engagement of CD28H on

NK cells induced Ca²⁺ flux with the agonistic mAb (clone 4–5), reflecting intracellular signaling, but not with the blocking anti-CD28H mAb (Ab from R&D Systems). Hence, CD28H must be targeted at the correct epitope to activate NK cells. This observation aligns with previous findings showing that the cross-linking of activating receptors at the correct epitope influences cell activation. For instance, targeting CD38 on human NK cells with the anti-CD38 clone IB4 induced Ca²⁺ mobilization, while the anti-CD38 clone IB6 did not [30], highlighting the importance of epitope specificity in receptor activation. It has been suggested that mAbs with membrane-distal epitopes might be better agonists than ligand-blocking mAbs whose epitopes are closer to the membrane. However, studies evaluating different anti-CD40 antibodies [31, 32] or agonistic capacities of different anti-OX40 mAbs shatter the previously mentioned dogma. Therefore, the relationship between epitope specificity and agonistic efficacy needs to be evaluated on a case-by-case basis.

Triggering CD28H activates NK cells, as shown by changes in their transcriptional profiles. Although fewer DEGs were observed in comparison to other studies [16, 17, 33], this discrepancy can be explained by the chosen kinetics and the different stimulation setups. Extra- and intracellular FACS staining further confirmed that NK-cell activation (i.e. 4-1BB and IFN- γ expression) occurred solely after overnight activation of CD28H with the agonistic mAb. Interestingly, supernatant from NK cells stimulated by platelet-derived growth factor D (PDGF-DD) NKp44 ligand, inhibits cancer epithelial cell line proliferation in an IFN- γ - and TNF- α -dependent manner and induces CADM1 (CRTAM ligand) and CD95 (Fas) expression in these cancer cell lines [33]. In our study, cell contact with target cells resulted in the secretion of IFN- γ and FAS-L by agonistic anti-CD28H-activated NK cells. While our study focused on hematopoietic cancer cell lines, it would also be interesting to further evaluate CD28H-triggered NK-cell effector functions in human epithelial cell lines, as with NKp44-activated NK cells [33]. This could provide valuable insights into the potential applications of CD28H-based immunotherapy in the context of solid tumors and their interactions with tumor cells of epithelial origin.

To our knowledge, our study is the first to evaluate the consequences of CD28H activation on NK-cell functions by comparing different mAbs. We demonstrated that the agonistic anti-CD28H mAb enhances NK-cell cytotoxicity toward K562, DAUDI, and Jurkat target cells. No synergy was observed when CD16 and CD28H were coengaged, as shown by both Ca²⁺ flux analysis and calcein assays, ruling out the synergistic effect of coengaging CD16 and CD28H. Although Zhuang and Long detected synergy between CD28H and CD16, the assays they used were quite different from our own, as they used a blocking anti-CD28H mAb

and *****p* < 0.0001. (C) HLA-A2 (black) and HLA-A2/HLA-E K562 cells (dark gray) were analyzed by FACS for their expression of HLA Class I with the pan anti-HLA Class I FITC clone W6.32 and an anti-HLA-A2 FITC and for their expression of HLA. (D) Freshly isolated NK cells were cultured overnight with the indicated mAbs prior to being seeded with the indicated target cells at a 1:2 E:T ratio. CD107a expression was analyzed by FACS. A representative FACS analysis is shown on the left. The percentages of CD107+ NK cells in 6 HDs from three independent experiments are shown on the right. Significance was calculated by two-way ANOVA followed by Dunn's multiple comparisons test. ns: nonsignificant, **p* < 0.05; ***p* < 0.01; ****p* < 0.001; *****p* < 0.0001.

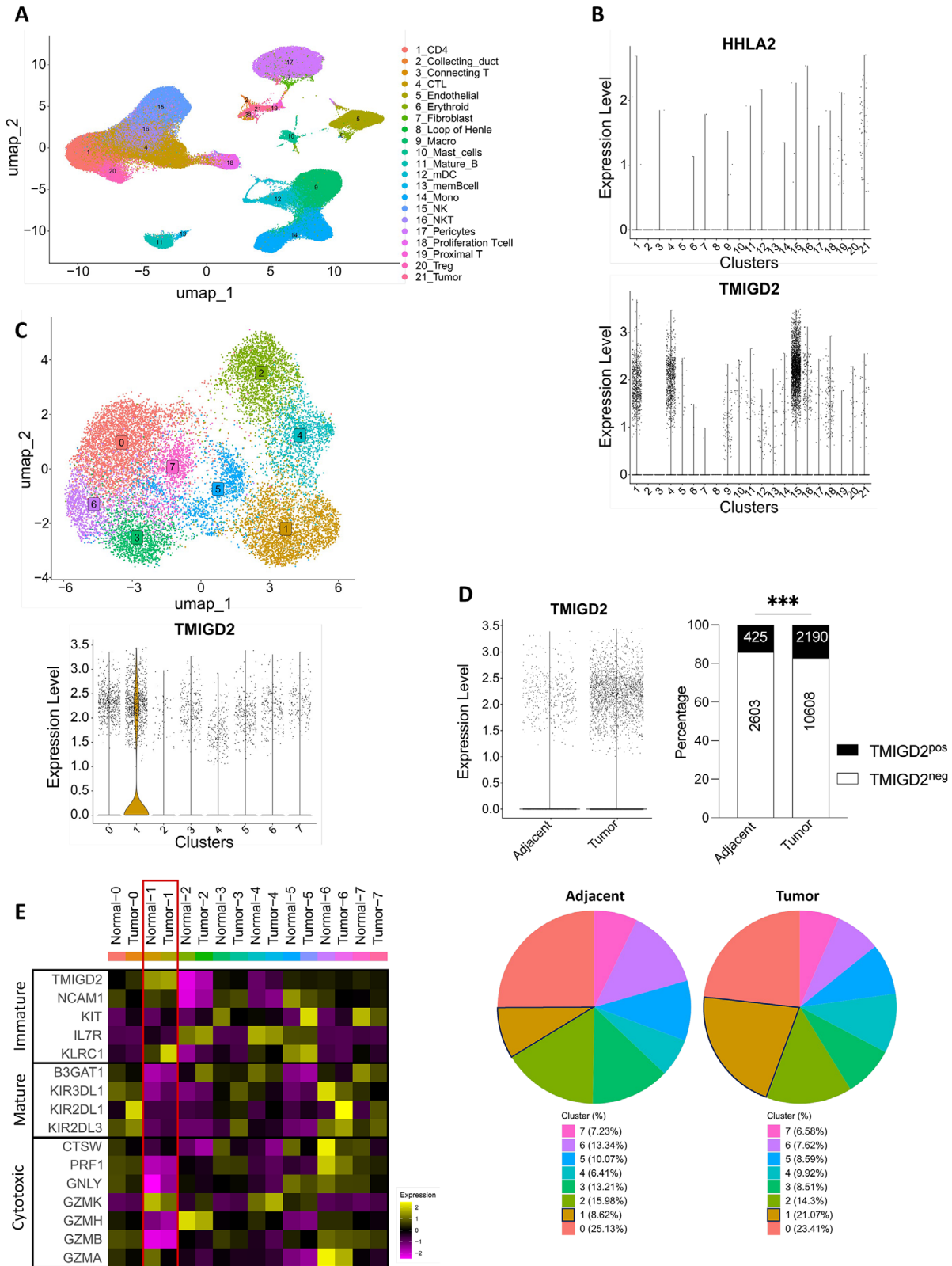


Figure 5. TMIGD2⁺ NK cells accumulate in ccRCC tumor samples compared with adjacent tissue samples. Publicly available scRNA-seq data from GSE178481 were used to evaluate the expression of our genes of interest in 15 primary ccRCC and 9 adjacent tissue samples. (A) Uniform manifold approximation and projection (UMAP) projections based on dimension reduction using PCA applied to the entire dataset (tumor and adjacent tissues) (after quality control) (n = 13,9976 cells). (B) A Violin plot showing the expression of TMIGD2 (upper panel) and HHLA2 (lower panel) in the 21 clusters shown in A (data are normalized and expressed in log1P). (C) UMAP plot of NK-cell subclustering (n = 15,826 cells) and violin plot showing

(a mouse monoclonal Ab) and an anti-CD16 mAb in redirected cytotoxicity assays with P815 murine target cells (also known as reverse ADCC) in which only these two molecules were engaged. Cotargeting of NKp46 and CD28H had synergistic effects on Ca^{2+} flux but not on cytotoxicity. This might be explained by the reductionist approach of the Ca^{2+} flux design experiment in which only one or two molecules are engaged. K562 cells are a more complex system since target cells carry other ligands and missing ligands (since K562 cells are HLA class I-negative cells) essential for NK-cell activation of effector functions; the additive value of coengaging CD28H and NKp46 by mAbs on NK cells fades over triggering CD28H activity alone, presumably because of target cell characteristics. The reductionist Ca^{2+} flux analysis approach, which detects massive Ca^{2+} influx only upon Ab binding followed by crosslinking (with a secondary Ab or by a cellular FcR as in reverse ADCC), does not predict the need for crosslinking of the receptor in its physiological function or in another experimental setup. Indeed, we show here that the agonistic anti-CD28H mAb needs to be crosslinked to allow rapid and massive Ca^{2+} flux, while when it is added “in solution” followed by the addition of target cells, it increases target cell killing. The same was true for anti-NKp46 and anti-CD16 antibodies, which were added overnight “in solution,” and both increased NK-cell cytotoxicity.

HHLA2 overexpression has been detected in various human cancers [2], including renal cell carcinomas, where its expression is mostly found in PDL-1^{neg} tumors. In rare tumors expressing both molecules, the HHLA2⁺ region does not overlap with that of PDL-1 [4]. Given that HHLA2 also binds to an inhibitory receptor on T-cells and NK92-MI cells, that is, KIR3DL3⁺ cells [4, 7, 34], we evaluated the cytotoxicity of NK cells activated with the agonistic anti-CD28H mAb to target cells expressing HHLA2. Our results demonstrated that HHLA2 expression on K562 target cells significantly decreases NK-cell degranulation, likely due to the engagement of the inhibitory ligand KIR3DL3, as observed by others using NK92-MI cells [4, 7]. Notably, we were not able to detect KIR3DL3 expression by FACS on resting NK cells or NK cells activated by the agonistic anti-CD28H mAb (data not shown). However, we demonstrated here that NK cells activated by the agonistic anti-CD28H mAb bypass, though not completely overcome, inhibitory signals mediated by HHLA2 and HLA-E. This observation is of particular interest for the therapeutic application of the anti-CD28H mAb in clinical settings.

The percentage of CD28H-expressing NK cells is lower in cancer tissues than in the peripheral blood cells of patients, as reported in a previous study [8]; however, HHLA2 expression is upregulated in numerous tumor cells; thus, CD28H-positive NK cells might still be activated within the tumor. Using a published scRNA-seq dataset of 15 primary ccRCC and 9 adjacent tissue sam-

ples [13], we showed that NK cells expressing TMIGD2 accumulate within tumors [35]. Although tumor-infiltrating TMIGD2^{pos} NK cells exhibit increased expression of NKG2A (*KLRC1*), we have shown that NK-cell stimulation with an agonistic anti-CD28H mAb bypasses the inhibitory signal mediated by HLA-E. Thus, these TMIGD2^{pos} NK cells may also respond to anti-CD28H mAb-based strategies.

In conclusion, our study revealed that the stimulation of CD28H by a properly selected mAb enhances NK-cell cytotoxicity against HHLA2^{neg} target cells and bypasses inhibitory signals such as those mediated by HHLA2 and HLA-E. These findings suggest that agonistic anti-CD28H mAbs could be a promising approach for enhancing antitumor immune responses.

Data limitations and perspectives

Several limitations of our study are worth mentioning. First, we and others [4, 7] have demonstrated that the expression of HHLA2 in K562 cells is protective; K562-HHLA2 cells are killed less frequently by NK cells than are K562-WT cells (Fig. 4B, Supporting Information Fig. S5D). Conversely, Zhuang and Long [6] reported increased killing frequencies of 721.221-HHLA2 and DAUDI-HHLA2 cells by NK cells compared with their WT counterparts. The nature of the transduced cells may explain this discrepancy, but it has not yet been addressed experimentally. Second, in vitro evaluation of renal cell carcinoma susceptibility to NK-cell and CD28H-activated NK-cell killing would have further emphasized our results. A-498 cells, a ccRCC cell line in which VHL is mutated, have been shown to be killed only by NK cells from patients with VHL-mutated ccRCC and not by NK cells from healthy donors [36]. Unfortunately, we do not have access to such biological samples. A deep analysis by immunohistology of NK cells within the ccRCC tumor and adjacent tissue samples will be needed to validate our observation of the scRNA-seq data. Finally, a limitation of our study is a lack of in vivo data due to the absence of the *HHLA2* and *TMIGD2* genes in mice and the lack of expression of CD28H on NKL and NK92 cells.

Materials and methods

Key resources

The materials used in this study are listed in Supporting Information Table S1.

the expression of *TMIGD2* in each NK-cell cluster (data are normalized and expressed in log_{1P}). (D) Violin plot showing the expression of *TMIGD2* in all NK cells from adjacent and tumor tissues (data are normalized and expressed in log_{1P}) is shown on the left, and the percentages of *TMIGD2*^{pos} (black) and *TMIGD2*^{neg} (white) NK cells in adjacent and tumor tissues are shown on the right (the numbers of NK cells are indicated for each group in the bar plot). Significance was calculated by a χ^2 test, *** $p < 0.001$. Pie charts representing the percentage of each NK-cell cluster in adjacent and tumor tissues. (E) Heatmap showing the expression of the corresponding genes used to define immature, mature, and cytotoxic NK cells. The color indicates gene expression calculated according to the formula detailed in the methods section.

Cells

Human peripheral blood mononuclear cells were isolated from blood collected at the Etablissement Français du Sang (EFS, CPDL-PLER-2018 180, and CPDL-PLER-2023 037) from healthy donors (HDs) with written informed consent. NK cells were isolated by negative selection with a Miltenyi NK-cell isolation kit, and the purity of the NK cells was analyzed by flow cytometry staining of CD56⁺CD3^{neg} cells and reached 90.64 ± 4% (Supporting Information Fig. S1A). Purified NK cells were cultured overnight at 37°C (5% CO₂) in complete medium (RPMI, Gibco), 10% fetal bovine serum (GE Healthcare HyClone), and 1% penicillin–streptomycin (Gibco, 1% glutamine) supplemented with 10 UI rhIL-2 (Cellgenix) and the indicated mAbs at 10 mg/mL. The K562 (ATCC CCL-243), DAUDI (ATCC CCL-213), and Jurkat tumor cell lines were cultivated in a complete medium. K562-HHLA2⁺ cells were generated in our laboratory by cloning the HHLA2 sequence (NP_009003) (synthesized by GenScript) into pHIV-Luciferase (Addgene plasmid #21375). Transduced K562 cells were subjected to FACS according to their HHLA2 expression. K562 HLA-A*02 and K562 HLA-A*02 HLA-E cells in which HLA-A2 leader peptide stabilized HLA-E expression [23] were a gift from Dr L. Vidard (Sanofi).

Characterization of the two anti-CD28H mAbs by bio-layer interferometry

The CD28H-HHLA2 interaction in the presence of the anti-CD28H mAbs (clones 4–5 and MAB83162 from R&D Systems) was evaluated by a Bio-Layer Interferometry BLItz System (Fortebio). First, the TMIGD2/CD28H His-tag recombinant protein (R&D Systems) was loaded on anti-HIS biosensors after washing with a specific Fortebio buffer. The biosensor was plunged in a 10 mg/mL anti-CD28H (clone 4–5 or MAB83162) solution. The biosensor was then washed prior to being plunged in a solution containing the HHLA2-Ig recombinant molecule (R&D Systems).

Production of the anti-CD28H monoclonal antibody clone 4–5

The hybridoma allowing the production of the hamster anti-human CD28H mAb (clone 4–5), generously provided by Dr. Lieping Cheng [5], was cultured in IMDM supplemented with 10% FBS. The antibodies in the supernatant were purified with a Hitrap protein G affinity column (GE Healthcare).

Calcium flux

One million NK cells were incubated with 5 μM Fura Red in calcium-free HBSS for 30 min at 37°C. NK cells were then incubated on ice for 30 min with primary antibodies. The cells were resuspended in HBSS supplemented with 10 mM HEPES, 1% BSA,

and 1 mM CaCl₂, and were acquired for 45 s with a FACS Celesta (BD Biosciences) prior to the addition of a cross-linker mixture to induce calcium flow. The cross-linker mixture was composed of 4 mg of anti-Armenian hamster antibody and 4 mg goat anti-mouse F(ab')₂ antibody (Supporting Information Table S1). Once cross-linked, the samples were vortexed and acquired on a FACS Celesta.

Staining procedure and flow cytometry assays

Cells (5 × 10⁵ per well) suspended in 200 μL of FACS buffer (1 × PBS, 1% BSA (Sigma–Aldrich), 0.1% azide (Sigma–Aldrich)) were plated in a V-bottom 96-well plate prior to centrifugation at 2500 rpm for 1 min. For extracellular staining, antibodies were added to each well, and the cells were incubated for 30 min on ice in the dark. For intracellular labeling, brefeldin A (5 mg/mL final) was added to the cell culture (i.e. NK ± K562) for 4 h prior to the use of the BD Cytofix/Cytoperm kit according to the manufacturer's protocol with the recommended volume of intracellular antibodies (anti-IFN-γ). Finally, the cells were washed twice before fluorescence acquisition with a FACS Celesta or an LSRII (BD Bioscience). The results were analyzed with FlowJo software (TreeStar). For receptor/ligand interactions, recombinant proteins were used at 5 μg/mL and added to the cells for 1 h at 37°C. After two washes, the cells were stained with an anti-human Fc secondary Ab for 30 min on ice in the dark.

RNA-seq preparation and analysis

Isolated NK cells were incubated overnight in a complete RPMI medium supplemented with 10 UI rhIL-2 and stimulated with or without 10 μg/mL anti-CD28H (clone 4–5) or the isotype control. Sixteen hours later, 2 million NK cells from each condition were washed in PBS, and the dry pellet was frozen at –80°C. The samples were then sent to QIAGEN Genomic Services for RNA extraction, library preparation, sequencing and read alignment. Briefly, total RNA extraction was performed using an RNeasy Mini kit (Qiagen) following the manufacturer's protocol. RNA quality was assessed using an Agilent TapeStation 4200 (Agilent Technologies), and only samples with high RNA integrity values were analyzed (RIN median = 8.1). Library preparation was performed using a TruSeq Stranded mRNA Sample Preparation Kit (Illumina Inc.) with 250 ng of total RNA. The mRNAs enriched with oligodT beads were fragmented via enzymatic fragmentation and used for cDNA synthesis before the double-stranded cDNA was purified (AMPure XP, Beckman Coulter). The cDNA was end-repaired, 3' adenylated and Illumina sequencing adaptors were ligated onto the fragment ends, and the library was purified (AMPure XP). The mRNA-stranded libraries were preamplified via PCR and subsequently purified (AMPure XP). The library size distribution was validated, and the library quality was inspected on a BioAnalyzer 4200 tape station (Agilent Technologies). Single-end sequencing was carried out on a NextSeq500 instrument (75 cycles) accord-

ing to the manufacturer's instructions (Illumina, Inc.). The data were aligned using TopHat (v 2.0.11) [37] and Cufflinks (v2.2.1) [38] with default settings and with the *Homo sapiens* GRCh37 reference genome. On average, 43.2 million reads were obtained for each sample, and the average genome mapping rate was 96.6%. Differential analysis of the transcript counts was performed using the *edgeR* R package [39]. Poorly expressed genes were filtered by keeping genes with at least 0.5 counts per million reads (cpm) in at least half of the samples. After normalization using the trimmed mean of M-values method, DEGs were identified using the quasi-likelihood F method. Genes with a Benjamini–Hochberg false discovery rate of less than 5% and a fold change (FC) greater than 2 were considered significantly differentially expressed. The biological significance of the DEGs was assessed using the *clusterProfiler* package [40]. GO categories enriched with a false discovery rate < 20% and with at least five genes were selected. The *GOplot* R package was used to represent the GO analysis results [41]. Redundant GO terms were reduced, and a z score, corresponding to the number of upregulated genes minus the number of downregulated genes divided by the square root of the number of genes in the category, was calculated. The RNA-seq data can be accessed under the GEO accession number GSE152269.

Protein secretion evaluated by Luminex

NK cells were incubated overnight with 10 µg/mL of the indicated mAbs. The next day, the NK cells were washed twice, counted, distributed at the indicated concentration, and incubated with 1×10^6 K562 target cells at a 1:1 effector:target (E:T) ratio for 6 h. The supernatant was frozen at -80°C . Luminex analysis was performed according to the manufacturer's protocol with the Human Custom Procartaplex 10 PLEX (PPX-10-MXRWE3N; Thermo Fisher).

Cytotoxicity assays

Calcein assays were performed as previously described [42]. Briefly, NK cells were cultured overnight in the presence of 10 µg/mL of the indicated mAbs. The next day, the NK cells were washed twice, counted, and distributed at the indicated concentrations. Target cells were incubated with 10 µM calcein and washed twice prior to being resuspended at 2×10^5 cells/mL in a complete medium containing 2.5 nM probenecid. NK and target cells were incubated for 4 h at 37°C (5% CO_2) with 20,000 labeled tumor cells at different E:T ratios. The supernatants were transferred to black 96-well plates (Greiner) and analyzed with a Spark plate reader (TECAN). Maximum and spontaneous release controls were set up in triplicate using 1% Triton X-100 (Sigma-Aldrich) or complete medium, respectively. The specific lysis was calculated as follows:

$$\frac{\text{Test release} - \text{spontaneous release}}{\text{Maximum release} - \text{spontaneous release}} \times 100$$

CD107a degranulation assays were performed as previously described [22]. Briefly, NK cells were cultured overnight with 10 µg/mL of the indicated mAb, washed, and then plated with target cells at the indicated E:T ratio with anti-CD107a antibody and Golgi STOP (containing monensin) for 2 h at 37°C and then acquired on a FACS Celesta (BD Bioscience). In some experiments, freshly isolated NK cells were used the next day for direct stimulation with 10 µg/mL of the indicated mAb and target cells for 2 h. The cells were then stained with an anti-CD107a mAb for 30 min at 4°C prior to acquisition on a FACS Celesta (BD Bioscience).

Processing of the published scRNA-Seq dataset

The raw count files from Alchahin et al. [13] (GSE178481) were downloaded. The classic pipeline for single-cell analysis in Seurat V4.3.0 was used to analyze the raw data from 15 ccRCC tumor samples (one of the 16 tumor samples available in the dataset was withdrawn because it was not classified as a ccRCC sample) and 9 adjacent tissue samples using the following steps: (1) cell selection, (2) filtering, and (3) normalization (with Harmony integration correction). A classic filtration step was performed by sample, with RNA features (or genes) detected between 200 and 4800 as well as mitochondrial RNA below 5%. Data normalization was performed to remove technical noise and adjust for differences in sequencing depth between samples. Feature selection was performed to identify highly variable genes that drive differences between cell types, and a PCA was performed to describe the variability of the whole gene expression dataset. Dimensionality reduction was then used to visualize the high-dimensional scRNA-seq data in two dimensions by the uniform manifold approximation and projection method using the first 20 PCs identified earlier. Clustering was then performed to group cells with similar gene expression profiles into discrete cell types. Louvain graph-based clustering with a 0.5 resolution resulted in 21 clusters (139976 cells: 111970 from tumor samples and 28006 from adjacent tissue samples). We used the same annotation determined by the authors of the paper where the raw data were available [<https://github.com/shenglinmei/ccRCC.analysis/>]. We selected the NK-cell cluster and performed the same pipeline described for the whole dataset, and we obtained 8 clusters (15826 cells: 12798 from tumor samples and 3028 from adjacent tissue samples) at a resolution of 0.5. The heatmaps in which color indicates gene expression were generated according to the following formula: $z \text{ score} = \frac{\bar{X}_X - \bar{X}_{\text{all}}}{\sigma_X}$, where \bar{X}_X represents the mean of the normalized expression value of gene A in cluster X, \bar{X}_{all} represents the mean of the normalized A gene expression value across all clusters, and σ_X represents the standard deviation of the normalized expression value of gene A in cluster X.

Statistical analysis

GraphPad Prism was used to perform the statistical analysis of the data: * < 0.05, ** < 0.01, *** < 0.001, **** < 0.0001.

Acknowledgements: This work was supported by a 2018 SANOFI iAward (FH) and the SATT (FH). Raphaëlle Leau was supported by the French minister of research BPI EFFI-CLIN PSPC grant ANR project KTD-innov (ANR-17-RHUS-0010) LabEX IGO ANR-11-LABX-0016. Pierre Duplouye was supported by a BPI EFFI-CLIN PSPC grant obtained from GB. Richard Danger was supported by the ANR project KTD-innov (ANR-17-RHUS-0010). This work was realized in the context of the LabEX IGO program supported by the National Research Agency through the investment of the future program ANR-11-LABX-0016. The authors thank Dr. LP Chen, for sharing the hybridoma and allowing the production of the anti-CD28H mAb clone 4–5 through MTA; Dr. L. Vidard, for fruitful and constructive discussions; and SANOFI, for the K562 HLA-A2 and K562 HLA-A2 HLA-E cells.

Conflict of interest: The authors declare no conflict of interest.

Author contributions: Fabienne Haspot conceived the study. Raphaëlle Leau, Pierre Duplouye, and Fabienne Haspot designed and supervised the experiments. Raphaëlle Leau, Pierre Duplouye, Virginie Huchet, Véronique Nerrière-Daguin, Mélanie Néel, Martin Morin, Bernard Martinet, Cécile Braudeau, and Fabienne Haspot performed the experiments. Raphaëlle Leau, Pierre Duplouye, Virginie Huchet, Véronique Nerrière-Daguin, Mélanie Néel, Martin Morin, Bernard Martinet, Richard Danger, Cécile Braudeau, Régis Josien, Gilles Blancho, and Fabienne Haspot analyzed the data and/or provided samples. Raphaëlle Leau, Pierre Duplouye, Richard Danger, and Fabienne Haspot wrote the manuscript.

Data availability statement: The data that support the findings of this study are available from the corresponding author upon reasonable request.

References

- Mager, D. L., Hunter, D. G., Schertzer, M. and Freeman, J. D., Endogenous retroviruses provide the primary polyadenylation signal for two new human genes (HHLA2 and HHLA3). *Genomics* 1999. 59: 255–263.
- Janakiram, M., Chinai, J. M., Fineberg, S., Fiser, A., Montagna, C., Medavarapu, R. et al., Expression, clinical significance, and receptor identification of the newest B7 family member HHLA2 protein. *Clin. Cancer Res.* 2015. 21: 2359–2366.
- Wang, B., Ran, Z., Liu, M. and Ou, Y., Prognostic Significance of potential immune checkpoint member HHLA2 in human tumors: a comprehensive analysis. *Front. Immunol.* 2019. 10: 1573.
- Bhatt, R. S., Berjis, A., Konge, J. C., Mahoney, K. M., Klee, A. N., Freeman, S. S. et al., KIR3DL3 is an inhibitory receptor for HHLA2 that mediates an alternative immunoinhibitory pathway to PD1. *Cancer Immunol. Res.* 2021. 9: 156–169.
- Zhu, Y., Yao, S., Iliopoulou, B. P., Han, X., Augustine, M. M., Xu, H. et al., B7-H5 costimulates human T cells via CD28H. *Nat. Commun.* 2013. 4: 2043–2043.
- Zhuang, X. and Long, E. O., CD28 homolog is a strong activator of natural killer cells for lysis of B7H7+ tumor cells. *Cancer Immunol. Res.* 2019. 7: 939–951.
- Wei, Y., Ren, X., Galbo Jr, P. M., Moerdler, S., Wang, H., Sica, R. A. et al., KIR3DL3-HHLA2 is a human immunosuppressive pathway and a therapeutic target. *Sci. Immunol.* 2021. 6.
- Crespo, J., Vatan, L., Maj, T., Liu, R., Kryczek, I. and Zou, W., Phenotype and tissue distribution of CD28H+ immune cell subsets. *Oncoimmunology* 2017. 6: e1362529.
- Palmer, W. H., Leaton, L. A., Codo, A. C., Crute, B., Roest, J., Zhu, S. et al., Polymorphic KIR3DL3 expression modulates tissue-resident and innate-like T cells. *Sci. Immunol.* 2023. 8: eade5343.
- Trundle, A. E., Hiby, S. E., Chang, C., Sharkey, A. M., Santourlidis, S., Uhrberg, M. et al., Molecular characterization of KIR3DL3. *Immunogenetics* 2006. 57: 904–916.
- Ramaswamy, M., Kim, T., Jones, D. C., Ghadially, H., Mahmoud, T. I., Garcia, A. et al., Immunomodulation of T- and NK-cell responses by a bispecific antibody targeting CD28 homolog and PD-L1. *Cancer Immunol. Res.* 2022. 10: 200–214.
- Zhuang, X. and Long, E. O., NK cells equipped with a chimeric antigen receptor that overcomes inhibition by HLA class I for adoptive transfer of CAR-NK cells. *Front. Immunol.* 2022. 13: 840844.
- Alchahin, A. M., Mei, S., Tsea, I., Hirz, T., Kfoury, Y., Dahl, D. et al., A transcriptional metastatic signature predicts survival in clear cell renal cell carcinoma. *Nat. Commun.* 2022. 13: 5747.
- Bryceson, Y. T., March, M. E., Ljunggren, H. G. and Long, E. O., Synergy among receptors on resting NK cells for the activation of natural cytotoxicity and cytokine secretion. *Blood* 2006. 107: 159–166.
- Boles, K. S., Barchet, W., Diacovo, T., Cella, M. and Colonna, M., The tumor suppressor TSLC1/NECL-2 triggers NK-cell and CD8+ T-cell responses through the cell-surface receptor CRTAM. *Blood* 2005. 106: 779–786.
- Campbell, A. R., Regan, K., Bhawe, N., Pattanayak, A., Parihar, R., Stiff, A. R. et al., Gene expression profiling of the human natural killer cell response to Fc receptor activation: unique enhancement in the presence of interleukin-12. *BMC Med. Genomics* 2015. 8: 66.
- Sabry, M., Zubiak, A., Hood, S. P., Simmonds, P., Arellano-Ballesterio, H., Cournoyer, E. et al., Tumor- and cytokine-primed human natural killer cells exhibit distinct phenotypic and transcriptional signatures. *Plos One* 2019. 14: e0218674.
- Romee, R., Lenvik, T., Wang, Y., Walcheck, B., Verneris, M. R. and Miller, J. S., ADAM17, a novel metalloproteinase, mediates CD16 and CD62L shedding in human NK cells and modulates IFN γ responses. *Blood* 2011. 118: 2184–2184.
- Ndhlovu, L. C., Lopez-Vergès, S., Barbour, J. D., Jones, R. B., Jha, A. R., Long, B. R. et al., Tim-3 marks human natural killer cell maturation and suppresses cell-mediated cytotoxicity. *Blood*. 2012;119: 3734–3743.
- Zamai, L., Ahmad, M., Bennett, I. M., Azzoni, L., Alnemri, E. S. and Perussia, B., Natural killer (NK) cell-mediated cytotoxicity: differential use of TRAIL and Fas ligand by immature and mature primary human NK cells. *J. Exp. Med.* 1998. 188: 2375–2380.
- Palmer, W. H., Leaton, L. A., Codo, A. C., Hume, P. S., Crute, B., Stone, M. et al., Polymorphic KIR3DL3 expression modulates tissue-resident and innate-like T cells. *Biorxiv* 2022. 2022.08.17.503789.
- Alter, G., Malenfant, J. M. and Altfeld, M., CD107a as a functional marker for the identification of natural killer cell activity. *J. Immunol. Meth.* 2004. 294: 15–22.

- 23 Lee, N., Llano, M., Carretero, M., Ishitani, A., Navarro, F., López-Botet, M. et al., HLA-E is a major ligand for the natural killer inhibitory receptor CD94/NKG2A. *Proc. Nat. Acad. Sci.* 1998. **95**: 5199–5204.
- 24 Tang, F., Li, J., Qi, L., Liu, D., Bo, Y., Qin, S. et al., A pan-cancer single-cell panorama of human natural killer cells. *Cell* 2023. **186**: 4235–4251. e20.
- 25 Cao, Y., Wang, X., Jin, T., Tian, Y., Dai, C., Widarma, C. et al., Immune checkpoint molecules in natural killer cells as potential targets for cancer immunotherapy. *Signal Transduct. Target. Ther.* 2020. **5**: 250.
- 26 Pinto, S., Pahl, J., Schottelius, A., Carter, P. J. and Koch, J., Reimagining antibody-dependent cellular cytotoxicity in cancer: the potential of natural killer cell engagers. *Trends Immunol.* 2022. **43**: 932–946.
- 27 Gauthier, L., Morel, A., Anceriz, N., Rossi, B., Blanchard-Alvarez, A., Grondin, G. et al., Multifunctional natural killer cell engagers targeting NKG2A trigger protective tumor immunity. *Cell*. 2019. **177**: 1701–1713. e16.
- 28 Watkins-Yoon, J., Guzman, W., Oliphant, A., Haserlat, S., Leung, A., Chotzin, C. et al., CTX-8573, an innate-cell engager targeting BCMA, is a highly potent multispecific antibody for the treatment of multiple myeloma. *Blood* 2019. **134**: 3182–3182.
- 29 André, P., Denis, C., Soulas, C., Bourbon-Caillet, C., Lopez, J., Arnoux, T. et al., Anti-NKG2A mAb is a checkpoint inhibitor that promotes anti-tumor immunity by unleashing both T and NK cells. *Cell*. 2018. **175**: 1731–1743. e13.
- 30 Mallone, R., Funaro, A., Zubiaur, M., Baj, G., Ausiello, C. M., Tacchetti, C. et al., Signaling through CD38 induces NK cell activation. *Int. Immunol.* 2001. **13**: 397–409.
- 31 Yu, X., Chan, H. T. C., Orr, C. M., Dadas, O., Booth, S. G., Dahal, L. N. et al., Complex interplay between epitope specificity and isotype dictates the biological activity of anti-human CD40 antibodies. *Cancer Cell* 2018. **33**: 664–675. e4.
- 32 Zhang, P., Tu, G. H., Wei, J., Santiago, P., Larrabee, L. R., Liao-Chan, S. et al., Ligand-blocking and membrane-proximal domain targeting anti-OX40 antibodies mediate potent T cell-stimulatory and anti-tumor activity. *Cell Reports* 2019. **27**: 3117–3123. e5.
- 33 Barrow, A. D., Edeling, M. A., Trifonov, V., Luo, J., Goyal, P., Bohl, B. et al., Natural killer cells control tumor growth by sensing a growth factor. *Cell* 2018. **172**: 534–548. e19.
- 34 Zhao, R., Chinai, J. M., Buhl, S., Scandiuizzi, L., Ray, A., Jeon, H. et al., HHLA2 is a member of the B7 family and inhibits human CD4 and CD8 T-cell function. *Proc. Nat. Acad. Sci.* 2013. **110**: 9879–9884.
- 35 Böttcher, J. P., Bonavita, E., Chakravarty, P., Blees, H., Cabeza-Cabrero, M., Sammiceli, S. et al., NK cells stimulate recruitment of cDC1 into the tumor microenvironment promoting cancer immune control. *Cell* 2018. **172**: 1022–1037. e14.
- 36 Trotta, A. M., Santagata, S., Zanotta, S., D'Alterio, C., Napolitano, M., Rea, G. et al., Mutated Von Hippel-Lindau-renal cell carcinoma (RCC) promotes patients specific natural killer (NK) cytotoxicity. *J Exp Clin Cancer Res* 2018. **37**: 297.
- 37 Kim, D., Pertea, G., Trapnell, C., Pimentel, H., Kelley, R. and Salzberg, S. L., TopHat2: accurate alignment of transcriptomes in the presence of insertions, deletions and gene fusions. *Genome Biol* 2013. **14**: R36.
- 38 Trapnell, C., Roberts, A., Goff, L., Pertea, G., Kim, D., Kelley, D. R. et al., Differential gene and transcript expression analysis of RNA-seq experiments with TopHat and Cufflinks. *Nat Protoc* 2012. **7**: 562–578.
- 39 Lun, A. T. L., Chen, Y. and Smyth, G. K., It's DE-licious: a recipe for differential expression analyses of RNA-seq experiments using quasi-likelihood methods in edgeR. *Meth. Mol. Biol. Clifton N J.* 2016. **1418**: 391–416.
- 40 Hochberg, Y. and Benjamini, Y., More powerful procedures for multiple significance testing. *Statist. Med.* 1990. **9**: 811–818.
- 41 Walter, W., Sánchez-Cabo, F. and Ricote, M., GPlot: an R package for visually combining expression data with functional analysis. *Bioinformatics* 2015; **31**: 2912–2914.
- 42 Vidard, L., Dureuil, C., Baudhuin, J., Vescovi, L., Durand, L., Sierra, V. et al., CD137 (4-1BB) engagement fine-tunes synergistic IL-15- and IL-21-driven NK cell proliferation. *J. Immunol.* 2019. **203**: 676–685.

Abbreviations: **ccRCC:** clear cell renal cancer cells · **DEGs:** differentially expressed genes · **GO:** gene ontology · **HDs:** healthy donors · **HHLA2:** HERV-H LTR-associating 2 · **mAbs:** monoclonal antibodies · **scRNA-seq:** single-cell RNA sequencing

Full correspondence: Dr. Fabienne Haspot, Center for Research in Transplantation and Translational Immunology, Nantes Université, INSERM, Center for Research in Transplantation and Translational Immunology, UMR 1064, F-44000, Nantes, France
e-mail: fabienne.haspot@univ-nantes.fr

Current address: Pierre Duplouye, Cancer Research Center of Lyon, Centre Léon Bérard, UMR INSERM 1052/CNRS 5286, F-69373, Lyon, France.

Received: 14/11/2023

Revised: 25/7/2024

Accepted: 26/7/2024

Accepted article online: 28/7/2024